Experimental and Analytical Study of Additively Manufactured Ti-TiB Metal Matrix Composite on Directional Isothermal-Fatigue

Thevika Balakumar * , Reza A. Riahi , Afsaneh Edrisy

Posted Date: 7 March 2024

doi: 10.20944/preprints202403.0401.v1

Keywords: Additive manufacturing; directional fatigue; isothermal fatigue; Ti–TiB MMC; Paris' equation; modified Paris' equation

 doi:10.20944/preprints202403.0401.v1

Article

Experimental and Analytical Study of Additively Manufactured Ti-TiB Metal Matrix Composite on Directional Isothermal-Fatigue

T. Balakumar *, R. Riahi and A. Edrisy

Department of Mechanical, Automotive & Materials Engineering, University of Windsor, Windsor, Ontario, N9B 3P4, Canada

* Correspondence: balakumt@uwindsor.ca

Abstract: Additive manufacturing (AM) techniques are widely investigated for the cost-effective use of titanium (Ti) alloys in various aerospace applications. One of the AM techniques developed for such applications is plasma transferred arc solid free-form fabrication (PTA-SFFF). Materials manufactured through AM techniques often exhibit anisotropies in mechanical properties due to the layer-by-layer material build. In this regard, the present study investigates the isothermal directional fatigue of Ti-TiB metal matrix composite (MMC) manufactured by PTA-SFFF. This investigation includes rotating beam fatigue test, electron microscopy, and fatigue calculations. The fatigue experiments were performed at 350 ºC using specimen with the test axis oriented diagonally (45º) and parallel (90º) to the AM builds directions. The fatigue values from the current experiments along with literature data find that Ti MMC manufactured via PTA-SFFF exhibit fatigue anisotropy reporting highest strength in 90º and lowest in perpendicular (0º) AM build directions. Further, the electron microscopy investigations on 0º, 45º, and 90º AM build specimens reveal frequent TiB clusters in all three AM build directions and suggest that the spread of these TiB clusters play a role in fatigue anisotropy. Moreover, the fatigue calculations were performed using both the Paris' and recently reported modified Paris' equations. Comparison of R^2 values for these calculations show that modified Paris' equation predicts the fatigue life of AM Ti-TiB MMC more accurately than the Paris' equation.

Keywords: additive manufacturing; directional fatigue; isothermal fatigue; Ti–TiB MMC; Paris' equation; modified Paris' equation

1. Introduction

Use of additive manufacturing (AM) in aerospace component manufacturing and repair is on the rise due to its material and cost-saving capabilities, without compromising the mechanical properties of the components. According to the European patent office publication [1], aerospace is the largest field among the transportation industry that uses AM to manufacture lightweight components, thereby aiding in the reduction of weight, fuel consumption, and emissions. In this regard, titanium (Ti) alloys are often selected as candidate materials in such applications due to their high specific strength and good corrosion resistance at elevated temperatures [2,3].

When considering Ti alloy use in aerospace industry, they are often utilized in constructing airframe parts, and gas turbine engines parts [2–5]. In order to meet the present day demand for improved mechanical properties and also to manufacture low cost Ti alloys, various Ti metal matrix composites (MMC) with particle reinforcements of borides, carbides, nitrides, and graphene were studied [6–8]. In this regard, it was reported in [9–11] that Ti MMCs with TiB show great promise as TiB exhibits high elastic modulus and thermal stability.

One of the disadvantages of considering AM over conventional manufacturing processes is that the materials manufactured through AM techniques often show anisotropic properties with respect

 doi:10.20944/preprints202403.0401.v1

to the AM build directions due to their layer-by-layer material build technique and the microstructure and defects associated with it [12–14]. In this context, often Ti-6Al-4V alloys manufactured through selective laser melting (SLM) and direct energy deposition (DED) were experimentally studied [15–18]. All three of these studies reported anisotropic fatigue strength of Ti-6Al-4V with respect to AM build directions. Further, they reported higher fatigue strengths when the test axes were along 0º [15,16], and 90º [17,18] to the AM direction.

The fatigue study in [15] investigated the directional fatigue strength of SLM Ti-6Al-4V. It utilized machined test specimens from SLM rods, testing them at room temperature on an electromagnetic resonance fatigue machine (QBG-25). The fatigue anisotropy observed in this study was attributed to the crystallographic texture and columnar grains in the SLM material build. In [16], as built AM Ti-6Al-4V samples via SLM were tested for directional fatigue strength on MTS 810 fatigue testing machine at room temperature. In this study, the observed anisotropic fatigue strengths at 0º and 90º angles to the AM directions were attributed mainly to the weak inter layer bonding. In [17], the directional fatigue study was carried out using both machined and as built SLM Ti-6Al-4V samples on a MTS load frame at room temperature. This study suggested that the aspects associated with SLM process such as porosity, microstructure and surface roughness could have contributed to the observed fatigue anisotropy. In [18], directional fatigue strength of Ti-6Al-4V manufactured by DED process was studied. In this work machined test specimens from DED block were tested on an Instron 8801-100 kN hydraulic servo fatigue tester at room temperature. This study attributed the crystallographic texture and alpha colonies with directional characteristics to the fatigue anisotropy.

In the present work, directional isothermal-fatigue of Ti-TiB MMC manufactured by plasma transferred arc solid free-form fabrication (PTA-SFFF) was investigated at 350ºC in three AM build orientations: 0º (test axis is parallel to), 45º (test axis is 45º to), and 90º (test axis is perpendicular to) AM direction. Among these three AM directions, experimental data in 45º and 90º AM build directions were collected in the present study. The data in 0º AM build direction at 350ºC was extracted from the current authors' previous experimental work reported in [19]. Further, the fatigue data for the current work was collected using a rotating beam fatigue (RBF) tester following the experimental setup described in [19]. Moreover, to investigate influence of TiB on crack initiations, propagations, and the overall directional fatigue strength of the Ti-TiB MMC, electron microscopy images were collected from polished as well as fatigue fractured specimens. In addition to the current fatigue and electron microscopy experimental work, an analytical investigation on the fatigue life predictability of the modified Paris' equation described in [19] was tested against general Paris' equation using current and literature [19] experimental data.

The above-described directional isothermal-fatigue investigation of AM Ti-TiB MMC are further detailed in the remainder of this manuscript under Sections 2–4. In Section 2, specimen orientations, current experimental results on isothermal fatigue in 45º and 90º AM build directions, and electron microscopy images are provided. In Section 3, the experimental findings on directional fatigue (in 0º, 45º, and 90º AM build directions), and Ti-TiB MMC fracture characteristics at 350 º are analysed. This section also presents fatigue calculations associated with the current experimental data using Paris' and modified Paris' equations. Finally, the findings of the current experimental and analytical work are presented in Section 4.

2. Specimen Orientations and Experimental Results

The present work is a continuation of the research work presented in [19]. As such, the compositional information of the Ti-TiB MMC, the dimensions of the fatigue specimens, the sample preparation procedures, and the RBF setup can be found in [19]. However, in contrast to the specimens used in [19], which were machined to have their fatigue test axis perpendicular to the AM build direction (0º), the specimens for the present study were machined in 45º and 90º AM build direction as shown in Figure 1.

 doi:10.20944/preprints202403.0401.v1

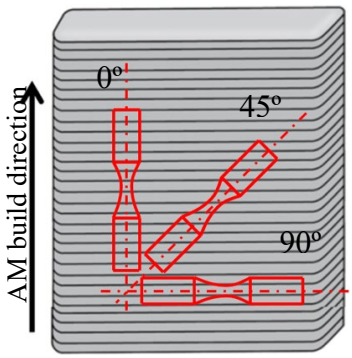

Figure 1. Schematic of three different fatigue specimen axis orientations (0º, 45º, and 90º) with respect to the AM build direction that were considered in the present study.

The current experimental fatigue data for AM Ti-TiB MMC at 350 ºC in 45º, and 90º AM build directions along with fatigue data from the literature [19] in 0º AM build direction at 350 ºC are presented in Figure 2.

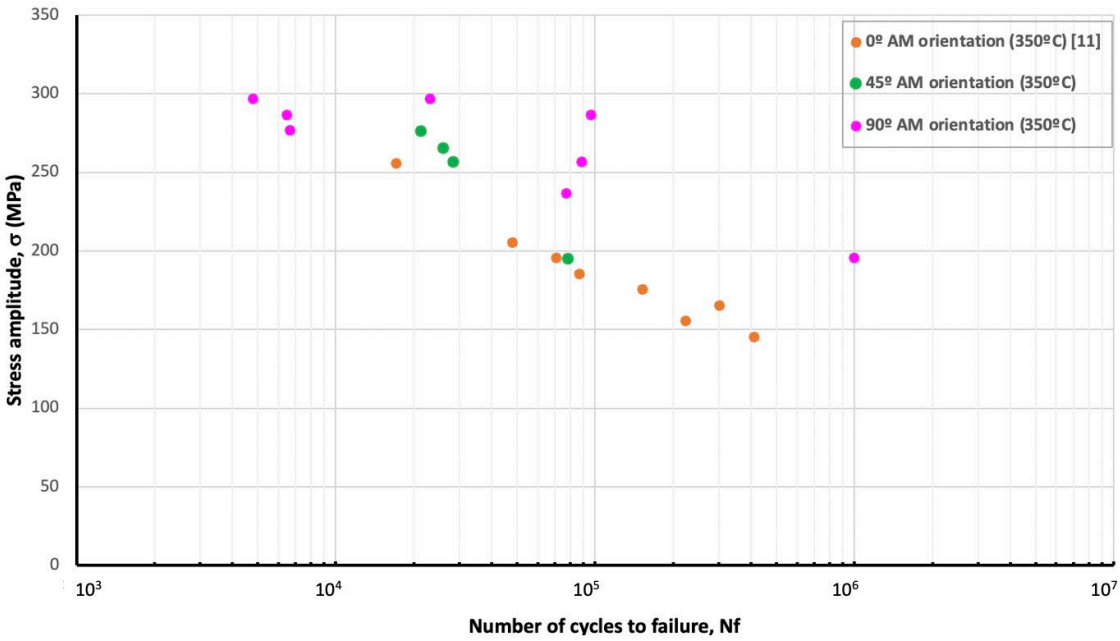

Figure 2. S-N plots for the isothermal (350 ºC) fatigue strengths of AM Ti-TiB MMC in 0º, 45º, and 90º AM build directions.

The electron microscopy images collected from the fractured fatigue specimens as well as from polished and etched specimens with 0º, 45º, and 90º AM build directions are given in Figures 3–6. The specimens that were polished and etched were cut in such a manner that representative cross sections of the fatigue specimens with 0º, 45º, and 90º AM builds could be studied. The low magnification (28x) back scattered electron (BSE) images in Figure 3 show the complete fracture surfaces of fractured fatigue specimens with 45º and 90º AM build orientations. The high magnification (in the range of 600x-8000x) BSE images in Figure 4 show various fracture characteristics that were observed in 45º and 90º AM orientation samples.

 doi:10.20944/preprints202403.0401.v1

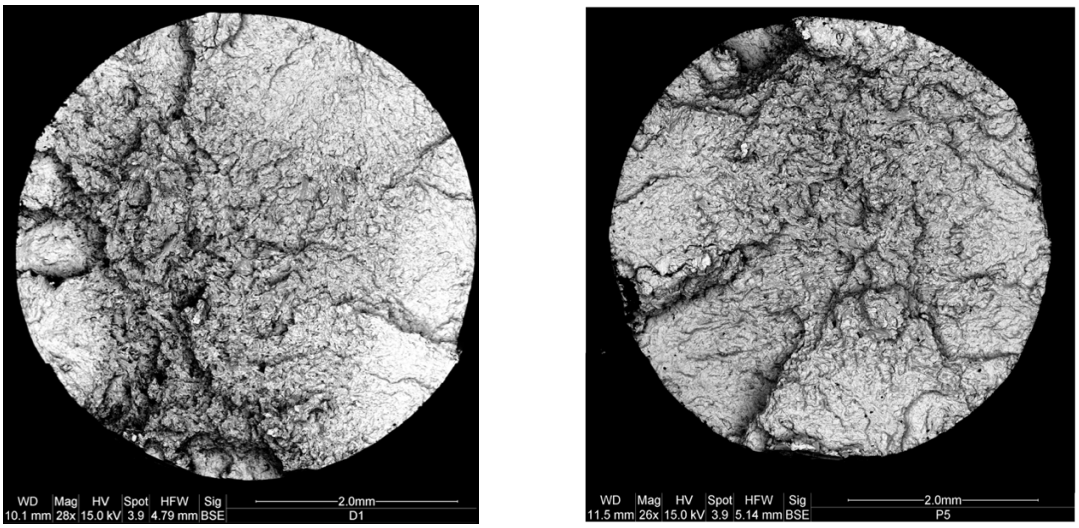

(a) (b)

Figure 3. BSE images of (a) a 45º AM build direction specimen fractured at the applied stress of σ=256.5 MPa and at 350ºC (b) a 90º AM build direction specimen fractured at the applied stress of σ=296.5 MPa and at 350ºC.

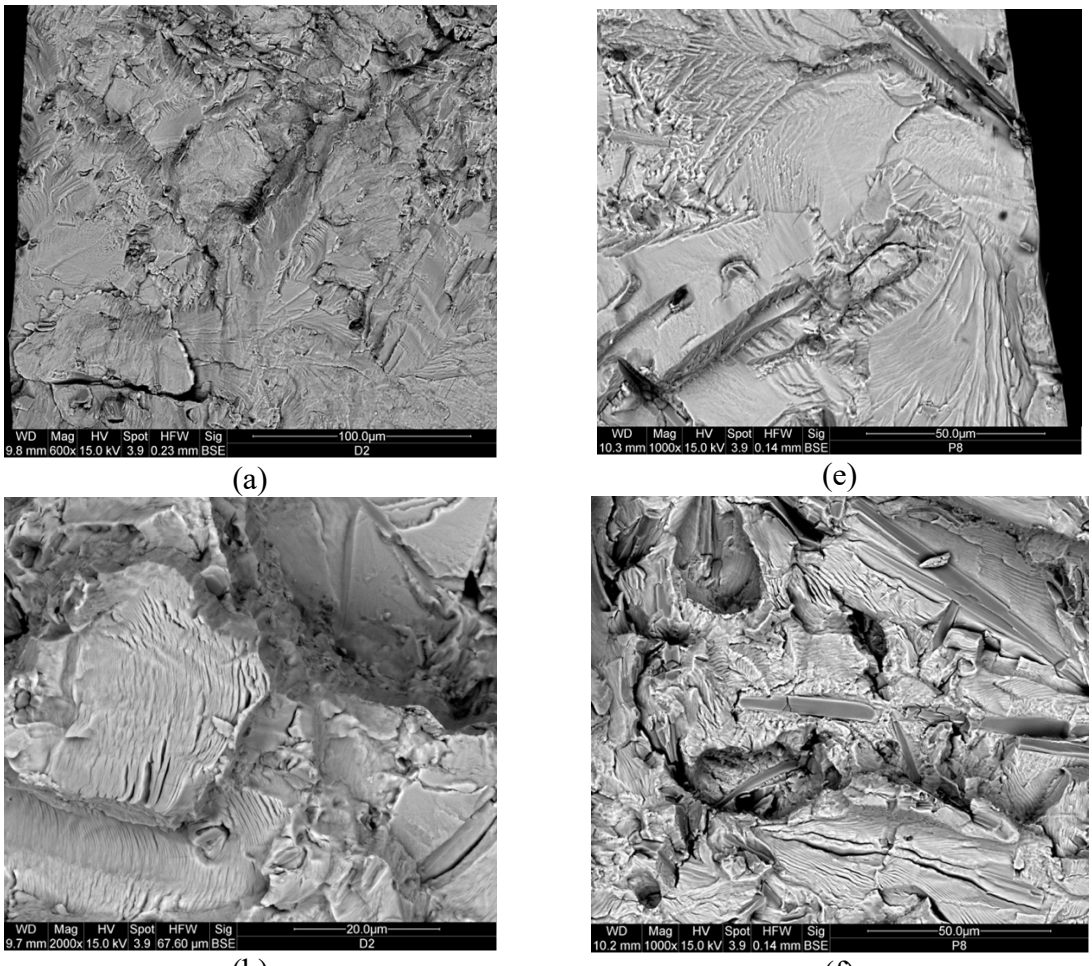

(a) (e)

(b) (f)

 doi:10.20944/preprints202403.0401.v1

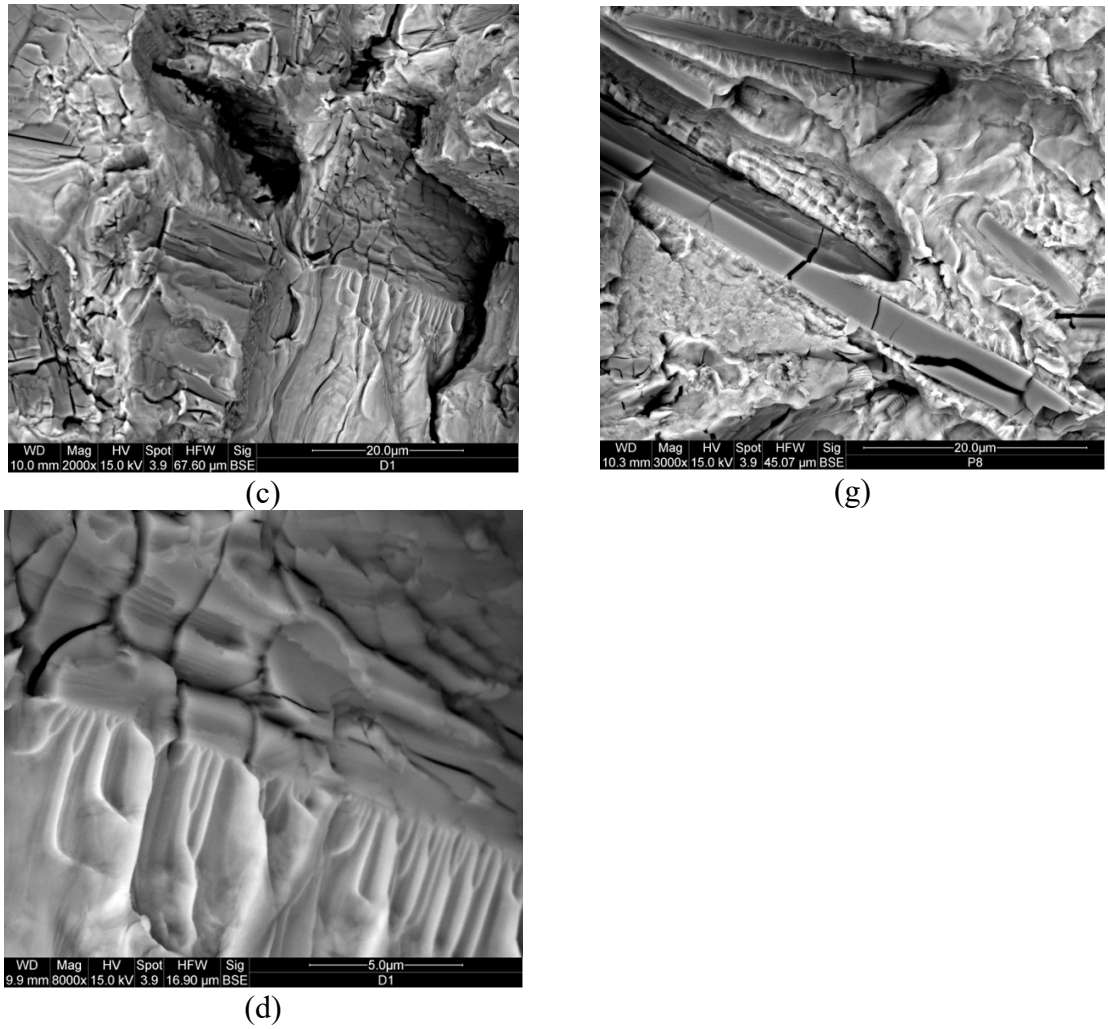

Figure 4. BSE images of 45º AM orientation samples that show fracture characteristics such as: (a) alpha Ti matrix cleavage (b) striations in alpha Ti matrix (c) fractured TiB particles surrounded by features of blocked pores during fracture (d) an enlarged portion of (c) showing striations in broken TiB particle, and BSE images of 90º AM orientation samples that show fracture features such as: (e) alpha Ti matrix cleavage (f) striations in alpha Ti matrix (g) fractured TiB particles surrounded by features of blocked pores during fracture.

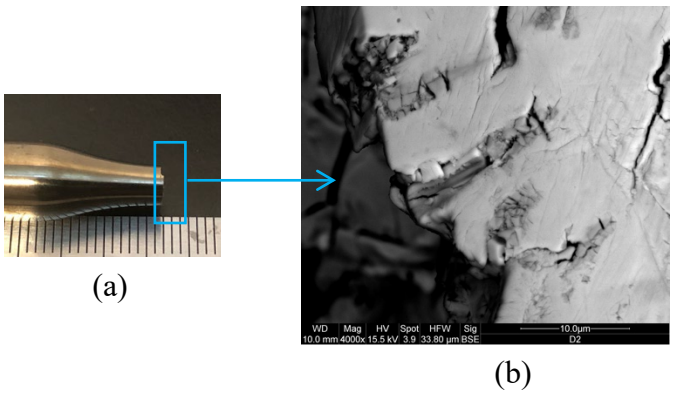

Figure 5. (a) one half of a fatigue fractured test specimen (b) BSE image of the peripheral surface of the fractured fatigue specimen shown in (a).

 doi:10.20944/preprints202403.0401.v1

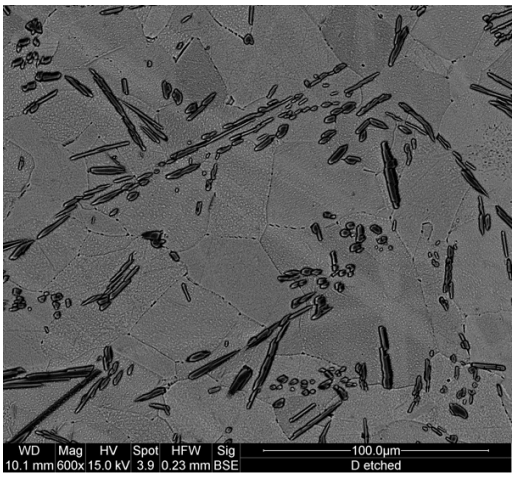

(a)

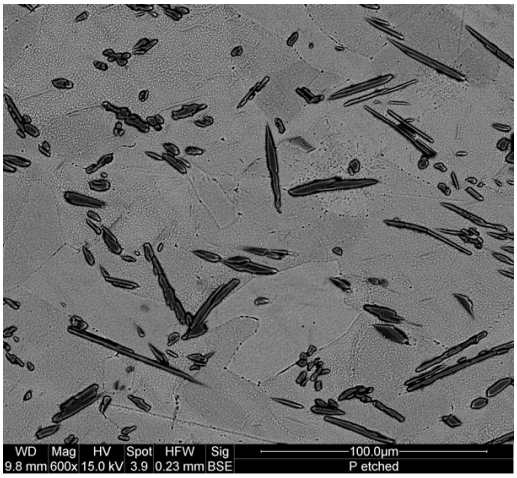

(b)

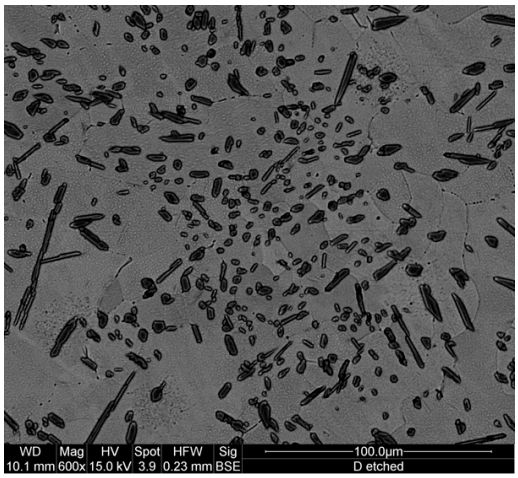

(c)

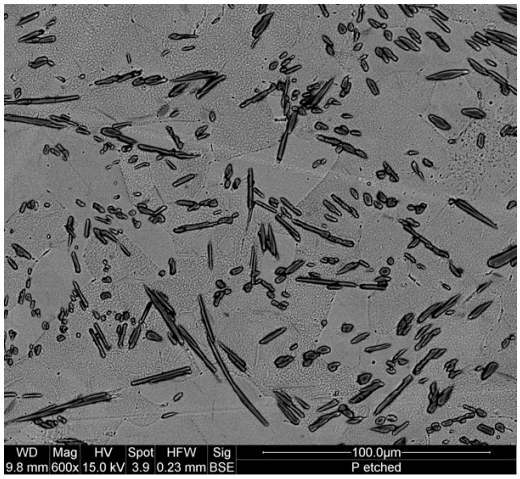

(d)

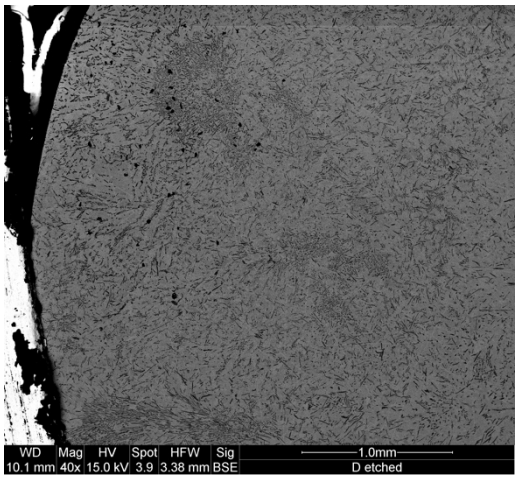

(e)

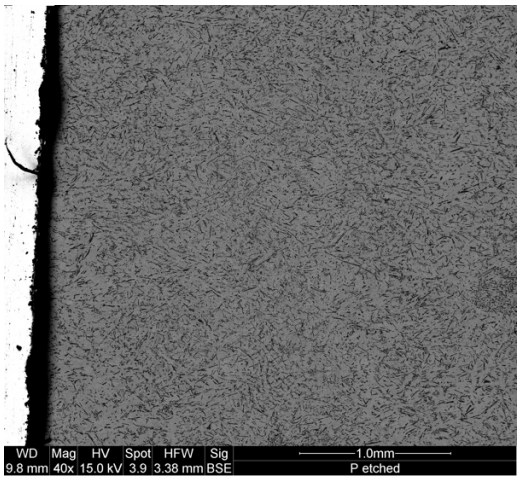

(f)

 doi:10.20944/preprints202403.0401.v1

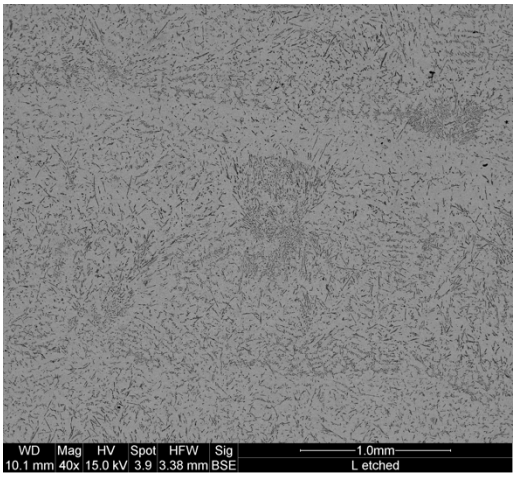

(g)

Figure 6. The pairs of BSE images that show (a)-(b) a random distribution of TiB (c)-(d) an occasional cluster of TiB (e)-(f) low magnification images that show general spread of TiB in 45º and 90º AM orientation respectively and (g) low magnification images that show general spread of TiB in 0º AM orientation.

Figure 5 comprises (a) an image of peripheral surface of a fractured fatigue specimen and (b) an electron microscopy image along the fracture that shows extensive cracks in TiB. Since the TiB particles showed significant fracture, samples with 0º, 45º and 90º AM build orientations were polished and etched and observed under electron microscope to find how these particles are distributed in the Ti matrix. Samples in all three AM orientations showed similar distribution of TiB and the SEM images obtained from 45º and 90º AM build orientations are given in Figure 6.

3. Analysis

The isothermal fatigue plots in Figure 2 show that Ti-TiB MMC manufactured by PTA-SFFF exhibit fatigue anisotropy with the highest strength in 90º, moderate in 45º, and the lowest in 0º AM build orientations. Similar fatigue anisotropic results were observed in [17,18] in which the directional fatigue strengths of AM Ti-6Al-4V at room temperature were studied. Even though the fatigue plots in Figure 2 show fatigue anisotropy, specimens of all three AM build orientations exhibited similar fatigue fractures as shown in Figures 3 and 4 for 45º and 90º AM build specimens. Similar images for the 0º AM build specimen can be found in [19].

Further, the 45º and 90º AM build specimens exhibited more significant cleavage on the fractured surfaces compared to the 0º AM build specimen. Other fracture features such as dense striations in the alpha matrix (Figure 4b,f) and broken TiB particles were observed in all three AM build direction specimens. These dominant fracture features are given in Figure 4 for 45º and 90º AM build specimens and can be found in [19] for 0º AM build specimens. Moreover, TiB particles in all the tested specimens generally showed no striation marks when they were observed under SEM. However, it can be seen from Figure 4d that the higher magnification BSE image shows slight signs of striations in a TiB particle that is heavily surrounded by frill like features. This observation suggests that when the TiB particle blocks the moving pores, there is also a discernible degree of plastic deformation during fatigue.

When considering the impact of TiB particles on the fatigue fracture of the tested AM alpha Ti alloy containing TiB particles, it is evident from Figure 5b that the TiB particles undergo significant fracture in comparison to the alpha Ti matrix. Further, the SEM images in Figure 6 reveal several characteristics of TiB particles: (i) there is a slight preference for the TiB particles to sit near the grain boundaries of the alpha Ti grains (Figure 6a,b) (ii) there is a preference for them to be in and around alpha Ti grains with a particular texture (Figure 6a–d) (iii) clustering in the alpha Ti matrix (Figure 6e–g). These microscopic observations, along with those presented in Figures 3 and 5b showing major

 doi:10.20944/preprints202403.0401.v1

surface crack propagations and significant fractures in TiB particles, respectively, suggest that the distribution of TiB particles is a factor in determining the isothermal fatigue life of AM Ti-TiB MMC. For instance, when a surface crack initiates at a site with cluster of TiB particles it will propagate easily as they exhibit significant fracture compared to the alpha Ti matrix. Moreover, it can be seen from Figure 6g that, compared to the TiB particle distributions observed in materials built with 45º and 90º AM build orientations, as shown in Figure 6e and f respectively, the particle distribution in the 0º AM build material exhibits a distinct and layered pattern of TiB particles. From this observation of TiB particles in the alpha Ti matrix along with their significant fracture during fatigue, this study suggests that the distribution of TiB particles during PTA SFFF contributed to the observed fatigue anisotropy as well as for the lowest fatigue along 0º AM build compared to 45º and 90º.

In addition to the experimental fatigue and microscopy investigation presented in the present work, fatigue life calculations were carried out to evaluate the predictability of the modified Paris' equation presented in [19] by the authors of this manuscript. In this regard, directional isothermal fatigue of AM Ti-TiB MMC were calculated using Paris' (Equation (1)) and modified Paris' equations (Equation (2)).

$$N_{\mathrm{fP}} = \frac{a_{\mathrm{f}}^{1-\frac{n}{2}} - a_{\mathrm{i}}^{1-\frac{n}{2}}}{(1-\frac{n}{2})\beta\lambda^{n}(\Delta\sigma)^{n}\pi^{\frac{n}{2}}} \tag{1}$$

$$N_{\mathrm{fM}} = \frac{\left(\frac{a_{\mathrm{f}}}{\mu}\right)^{1-\frac{n}{2}} - a_{\mathrm{i}}^{1-\frac{n}{2}}}{(1-\frac{n}{2})\beta\lambda^{n}(\Delta\sigma)^{n}\pi^{\frac{n}{2}}} \tag{2}$$

In the above equations, N_{fP} and N_{fM} denote the calculated number of cycles to failure using Equations (1) and (2) respectively, λ denotes the stress intensity modification factor, β and n are material constants (that can found from the literatures), a_{i} and a_{f} refers the initial and final lengths of the surface crack, $\Delta\sigma$ is applied stress, and μ refers the number of major surface cracks propagated. As described in [19], the values of λ for the best prediction by Equations (1) and (2), denoted respectively by λ_{P}^{*} and λ_{M}^{*}, can be found through least square error minimization and their closed form expressions are respectively given by Equations (3) and (4).

$$\lambda_{\mathrm{P}}^{*} = \left[\frac{\sum_{j=1}^{z}\left(\frac{\gamma_{j\mathrm{P}}}{\delta_j}\right)^{2}}{\sum_{j=1}^{z}\left(\frac{\gamma_{j\mathrm{P}}}{\delta_j}\right)\cdot {N_{\mathrm{f}}}_{j}^{\mathrm{Exp}}}\right]^{\frac{1}{n}} \tag{3}$$

$$\lambda_{\mathrm{M}}^{*} = \left[\frac{\sum_{j=1}^{z}\left(\frac{\gamma_{j\mathrm{M}}}{\delta_j}\right)^{2}}{\sum_{j=1}^{z}\left(\frac{\gamma_{j\mathrm{M}}}{\delta_j}\right)\cdot {N_{\mathrm{f}}}_{j}^{\mathrm{Exp}}}\right]^{\frac{1}{n}} \tag{4}$$

where

$$\gamma_{j\mathrm{P}} = {a_{\mathrm{f}}}_{j}^{1-\frac{n}{2}} - {a_{\mathrm{i}}}_{j}^{1-\frac{n}{2}} \tag{5}$$

$$\delta_j = \left(1-\frac{n}{2}\right)\beta\pi^{\frac{n}{2}}\left(\Delta\sigma_j\right)^{n} \tag{6}$$

$$\gamma_{j\mathrm{M}} = \left(\frac{{a_{\mathrm{f}}}_{j}}{\mu_j}\right)^{1-\frac{n}{2}} - {a_{\mathrm{i}}}_{j}^{1-\frac{n}{2}} \tag{7}$$

for j number of experiments.

The evaluation of λ_{P}^{*} and λ_{M}^{*} in 0º, 45º and 90º AM build orientations, using Equations (1) and (2) are illustrated in Figure 7 and their values are tabulated in Table 1.

Preprints.org (www.preprints.org) | NOT PEER-REVIEWED | Posted: 7 March 2024 doi:10.20944/preprints202403.0401.v1

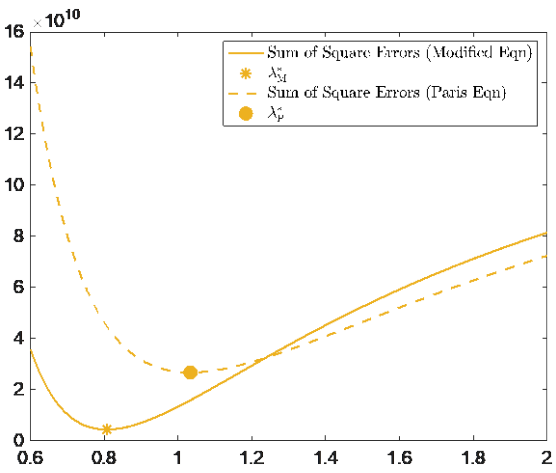

(a)

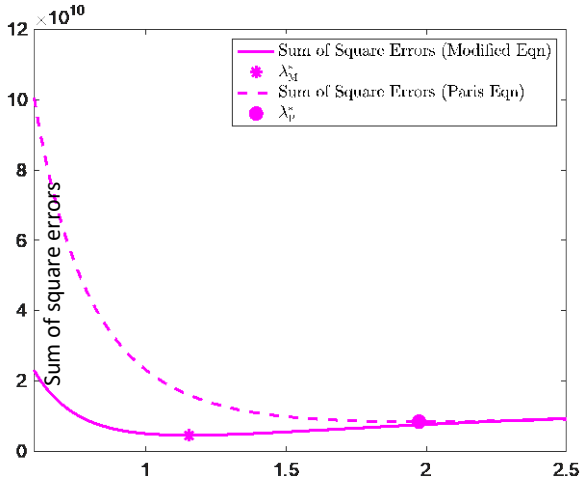

(c)

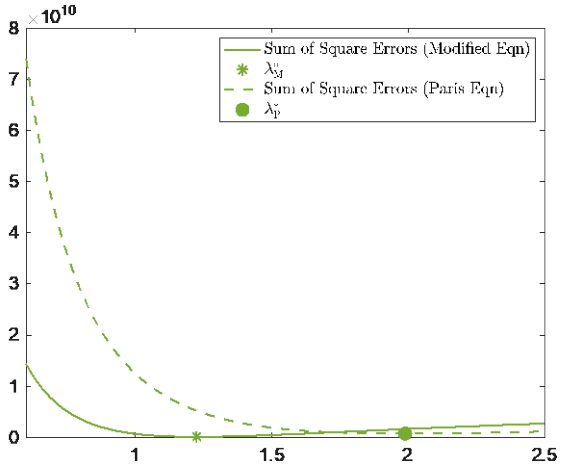

(b)

Figure 7. Plots for sum of square errors for calculations using Equations (1) and (2); (a) 0º (b) 45º and (c) 90º AM build orientations.

Table 1. Optimum stress intensity modification factors for 0º, 45º and 90º AM build orientations.

Specimen AM build orientation	λ_P^* for Equation (1)	λ_M^* for Equation (2)
0º	1.0333	0.8069
45º	1.9880	1.2247
90º	1.9737	1.1537

It can be noted from Table 1 that, the evaluated values for λ_P^* and λ_M^* for 45º and 90º AM build directions are almost the same and higher than that for 0º. Since the stress intensity modification factor, λ depends on the initial crack characteristics, the similar λ_P^* and λ_M^* values suggest that both 0º and 45º AM build specimens had similar crack initiation characteristics.

Moreover, using the values listed Table 1 for the modifications factors for 0º, 45º and 90º AM build orientations, and by taking the values for β=2 × 10^{-8}, and n=1.19, fatigue calculations were performed using Equations (1) and (2) and they are illustrated as S-N plots in Figure 8 along with

 doi:10.20944/preprints202403.0401.v1

experimental data from the current work as well as from the work reported in [19]. Furthermore, according to the description for λ given in [19], the initial surface crack length, a and the value of λ are inversely proportional. Hence, the lower values for λ_P^* and λ_M^* in Table 1 suggest larger surface crack initiations and lower fatigue values. This is evidenced by the smaller λ_P^* and λ_M^* values (Table 1) and lower fatigue strength (Figure 2) observed in 0º AM build directions compared to that in the 45º and 90º orientations. Further, the quality of these fatigue life calculations by Equations (1) and (2) were evaluated in terms of R^2 and tabulated in Table 2. It can be noted from Table 2 that the R^2 evaluated in relation to Equation (2) are superior to the ones for Equation (1). This finding suggests that the modified Paris' equation in Equation (2) make accurate fatigue life prediction than by Equation (1).

Table 2. R^2 values for the fatigue life of specimens with 0º, 45º and 90º AM build orientations calculated using Equations (1) and (2).

Specimen AM build orientation	R^2 for fatigue life calculation using Equation (1)	R^2 for fatigue life calculation using Equation (2)
0º	0.34	0.93
45º	0.67	0.96
90º	0.09	0.51

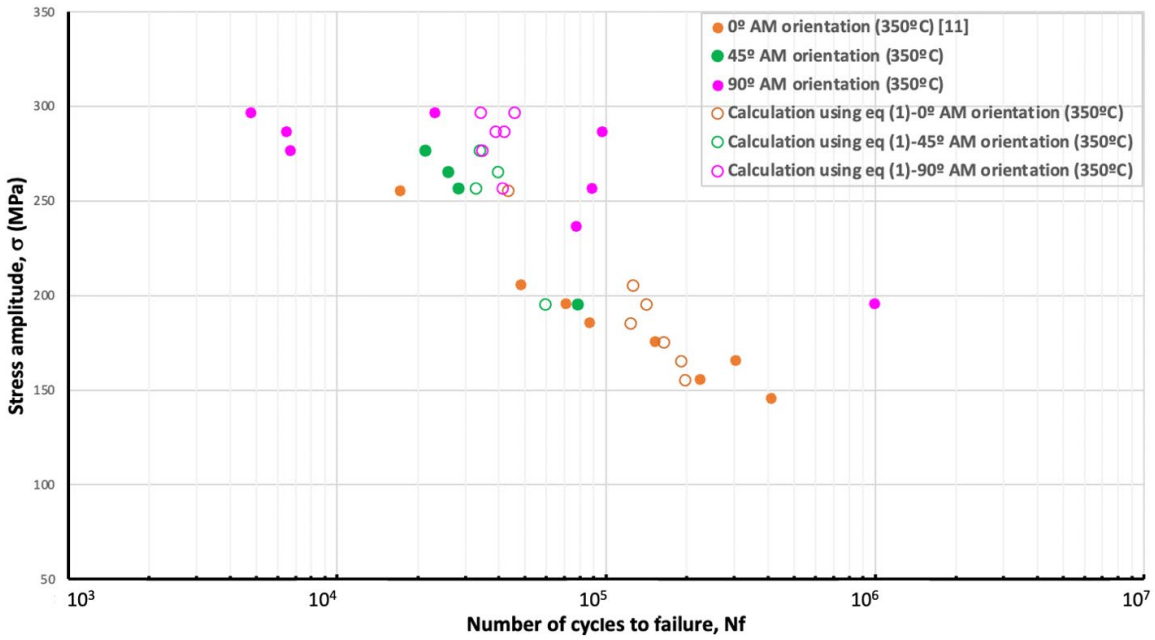

(a)

 doi:10.20944/preprints202403.0401.v1

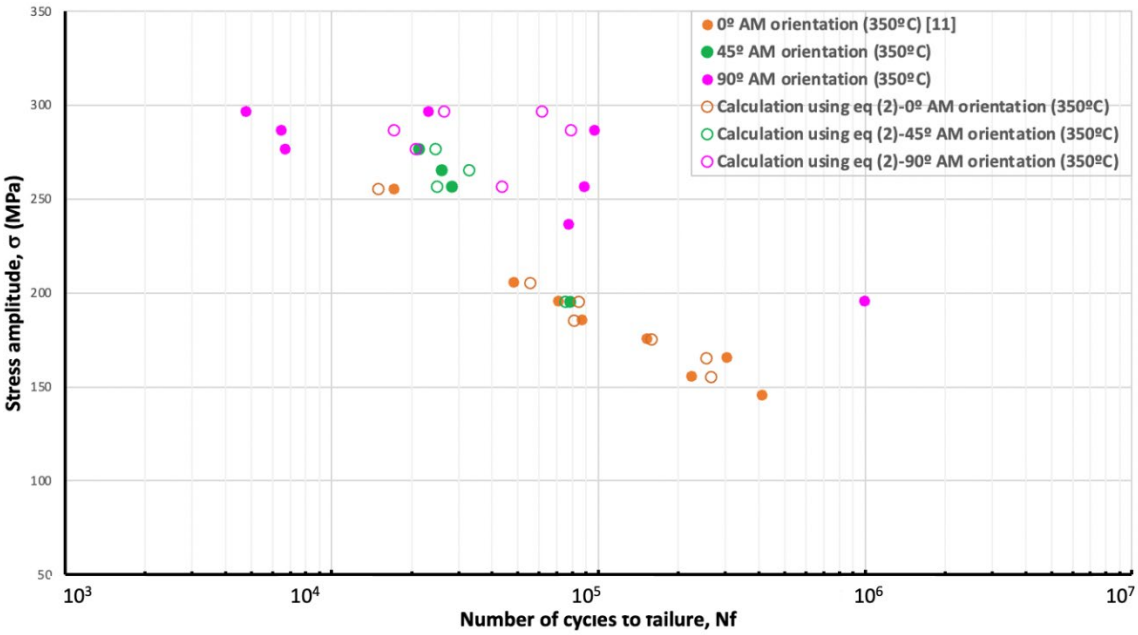

(b)

Figure 8. S-N plots for the specimens with 0º, 45º and 90º AM build orientations showing the experimental and (a) calculated data using Equation (1) (b) calculated data using Equation (2).

4. Conclusions

This study finds that the Ti-TiB MMC manufactured by plasma transferred arc solid free-form fabrication (PTA-SFFF) shows fatigue anisotropy. Among the three AM orientations considered in the present study, 90º AM build orientations exhibited better fatigue strength compared to those with 0º and 45º orientations.

Electron microscopy images obtained from the fractured specimen surfaces reveal that the final fracture in all three AM build directions occurred due to several large surface crack propagations. Also, these images show considerable cracks in TiB than Ti matrix. Further, the microscopy images obtained from the polished and etched specimen show frequent TiB clusters in in all three AM build directions. However, 0º specimen exhibited significantly different variation of TiB distribution, possibly between each AM build layers. These images also reveal that the TiB particles are preferably distributed along the matrix grain boundaries.

The fatigue calculations performed in the present work finds that the modified Paris' equation, that incorporates the contribution from the number of large surface crack propagations, accurately predict the fatigue life of Ti-TiB MMC manufactured via PTA-SFFF in all AM build directions. This finding suggests that this modified Paris' equation can be used for any AM material that exhibits significant number of surface crack propagations. Moreover, the lowest value calculated for the stress intensity modification factor for 0º AM build orientation supports the lowest experimental fatigue recordings and the significant TiB clusters in microscopy images. Furthermore, almost same values of stress intensity modification factor calculated for 45º, and 90º AM build directions. This finding suggests similar crack initiation characteristics in these AM build directions.

With regard to the crack initiation sites, no specific metallurgical factors identified in this work. Hence, an advanced image analysis that can reveal atomic level characteristics is required to investigate crack initiation. Furthermore, to investigate the crack propagation behaviour under isothermal fatigue of Ti-TiB MMC, more experiments are required.

Author Contributions: Conceptualization, Thevika Balakumar; Methodology, Thevika Balakumar; Validation, Thevika Balakumar and Reza A. Riahi; Formal analysis, Thevika Balakumar; Investigation, Thevika Balakumar; Data curation, Thevika Balakumar; Writing – original draft, Thevika Balakumar; Writing – review & editing,

 doi:10.20944/preprints202403.0401.v1

Thevika Balakumar and Reza A. Riahi; Visualization, Thevika Balakumar; Supervision, Reza A. Riahi and Afsaneh Edrisy; Project administration, Afsaneh Edrisy; Funding acquisition, Afsaneh Edrisy.

References

1. European Patent Office, "Innovation trends in additive manufacturing Patents in 3D printing technologies," Munich, Germany, 2023. [Online]. Available: https://link.epo.org/web/service-support/publications/en-additive-manufacturing-study-2023-full-study.pdf.
2. R. R. Boyer, "Titanium for aerospace: Rationale and applications," *Adv. Perform. Mater.*, vol. 2, no. 4, pp. 349–368, Oct. 1995, doi: 10.1007/BF00705316.
3. S. Gialanella and A. Malandruccolo, *Aerospace Alloys*. Cham: Springer International Publishing, 2020.
4. W. D. Brewer, R. K. Bird, and T. A. Wallace, "Titanium alloys and processing for high speed aircraft," *Mater. Sci. Eng. A*, vol. 243, no. 1–2, pp. 299–304, Mar. 1998, doi: 10.1016/S0921-5093(97)00818-6.
5. J. D. Cotton, L. P. Clark, and H. R. Phelps, "Titanium alloys on the F-22 fighter airframe," *Adv. Mater. Process.*, vol. 160, no. 5, pp. 25–28, 2002.
6. J. A. Hooker and P. J. Doorbar, "Metal matrix composites for aeroengines," *Mater. Sci. Technol.*, vol. 16, no. 7–8, pp. 725–731, Jul. 2000, doi: 10.1179/026708300101508414.
7. M. D. Hayat, H. Singh, Z. He, and P. Cao, "Titanium metal matrix composites: An overview," *Compos. Part A Appl. Sci. Manuf.*, vol. 121, pp. 418–438, Jun. 2019, doi: 10.1016/j.compositesa.2019.04.005.
8. D. K. Ammisetti and S. S. Harish Kruthiventi, "Recent trends on titanium metal matrix composites: A review," *Mater. Today Proc.*, vol. 46, pp. 9730–9735, 2021, doi: 10.1016/j.matpr.2020.08.732.
9. G. Singh and U. Ramamurty, "Boron modified titanium alloys," *Prog. Mater. Sci.*, vol. 111, p. 100653, Jun. 2020, doi: 10.1016/j.pmatsci.2020.100653.
10. Q. Li, S. Huang, Y. Zhao, Y. Gao, and U. Ramamurty, "Simultaneous enhancements of strength, ductility, and toughness in a TiB reinforced titanium matrix composite," *Acta Mater.*, vol. 254, p. 118995, Aug. 2023, doi: 10.1016/j.actamat.2023.118995.
11. S. Li *et al.*, "Towards high strengthening efficiency by in-situ planting nano-TiB networks into titanium matrix composites," *Compos. Part B Eng.*, vol. 245, p. 110169, Oct. 2022, doi: 10.1016/j.compositesb.2022.110169.
12. A. Charmi *et al.*, "Mechanical anisotropy of additively manufactured stainless steel 316L: An experimental and numerical study," *Mater. Sci. Eng. A*, vol. 799, p. 140154, Jan. 2021, doi: 10.1016/j.msea.2020.140154.
13. Y. Ren *et al.*, "Study of microstructural and mechanical anisotropy of 7075 Al deposits fabricated by cold spray additive manufacturing," *Mater. Des.*, vol. 212, p. 110271, Dec. 2021, doi: 10.1016/j.matdes.2021.110271.
14. Y. Kok *et al.*, "Anisotropy and heterogeneity of microstructure and mechanical properties in metal additive manufacturing: A critical review," *Mater. Des.*, vol. 139, pp. 565–586, Feb. 2018, doi: 10.1016/j.matdes.2017.11.021.
15. K. Chang *et al.*, "Microstructural feature and mechanical property in different building directions of additive manufactured Ti6Al4V alloy," *Mater. Lett.*, vol. 267, p. 127516, May 2020, doi: 10.1016/j.matlet.2020.127516.
16. W. Sun, Y. Ma, W. Huang, W. Zhang, and X. Qian, "Effects of build direction on tensile and fatigue performance of selective laser melting Ti6Al4V titanium alloy," *Int. J. Fatigue*, vol. 130, p. 105260, Jan. 2020, doi: 10.1016/j.ijfatigue.2019.105260.
17. P. Edwards and M. Ramulu, "Fatigue performance evaluation of selective laser melted Ti–6Al–4V," *Mater. Sci. Eng. A*, vol. 598, pp. 327–337, Mar. 2014, doi: 10.1016/j.msea.2014.01.041.
18. D. Tang, X. He, B. Wu, L. Dang, H. Xin, and Y. Li, "Anisotropic fatigue performance of directed energy deposited Ti-6Al-4V: Effects of build orientation," *Mater. Sci. Eng. A*, vol. 876, p. 145112, Jun. 2023, doi: 10.1016/j.msea.2023.145112.
19. T. Balakumar, R. Riahi, and A. Edrisy, "An investigation of fatigue of additively manufactured commercially pure Alpha–Ti alloy at 350 °C," *J. Mater. Res. Technol.*, vol. 26, pp. 7300–7311, Sep. 2023, doi: 10.1016/j.jmrt.2023.09.055.